Rock Mechanics and Rock Engineering
https://doi.org/10.1007/s00603-025-05162-8

ORIGINAL PAPER

Comparison of Measured and Modeled Casing Deformations of a Test Well in a Longwall Abutment Pillar

Peter Zhang[1] · **Daniel Su**[1] · **Bo Hyun Kim**[2] · **Evan Midler**[3]

Received: 30 May 2024 / Accepted: 25 November 2025

Abstract
Shale gas wells in longwall pillars are subjected to longwall-induced subsurface ground movements, and their stability has been a safety concern for both mining and gas operators. To understand the impact of longwall mining on gas wells in longwall chain pillars, a test well was drilled through an abutment pillar between two adjacent longwall panels to measure the casing deformations after each panel was mined. The longwall panels extracted the Pittsburgh Coal Seam under a depth of 177 m and were developed with a 3-entry system with 52-m-wide chain pillars and 366-m-wide panels. Casing deformations were measured with a 60-arm caliper and were observed with a downhole camera. Casing deformations were detected at ten locations with the maximum deformation being 8.2 cm at a 51-m depth after second panel mining. A FLAC3D model was set up to predict longwall-induced stresses and deformations in the test well casing. The model was validated with measured surface subsidence and longwall-induced pillar pressure. Both measurements and numerical modeling showed that the casing deformed because of relative horizontal displacements along distinct weak rock interfaces, and most of the casing deformations occurred after first panel mining. The casing deformations at the weak claystone interfaces were found to be confined within the thickness of the claystone layers. The knowledge of longwall-induced casing deformations gained from the test well was used to plan a mine-by case with five shale gas wells in chain pillars. These gas wells had production casings uncemented. The established FLAC3D model from the test well was used to predict intermediate casing deformations in the shale gas wells at the mine-by site. The predictions showed that the production casings were unaffected by longwall mining as the deformations in the intermediate casings were less than the open annulus between production and intermediate casing. The study of the test well led to a successful mine-by in which five shale gas wells in chain pillars were unaffected by the passing of the longwall faces and resumed production after being interrupted during the period of mine-by. The post-mining caliper survey showed no casing deformations in the uncemented production casings, and all the production casings passed pressure test. The FLAC3D model proved to be capable of predicting longwall-induced casing deformations with reasonable accuracy.

Highlights

- Casing deformations of a test well in longwall chain pillars under 177-m depth of cover were measured with a multi-finger caliper and predicted by FLAC3D modeling. Casing deformations occurred at distinct weak/strong rock interfaces due to relative horizontal displacements along the interfaces. Casing deformations occurred at the same locations for both first and second panel mining.
- Casing deformations in the five shale gas wells in longwall chain pillars in the same mining district were predicted using the established FLAC3D model from the test well study. As the predicted maximum casing deformation was less than the open annular space of 8.4 cm between the production and intermediate casing, no deformation was predicted in the uncemented production casings.
- With uncemented production casings, five shale gas wells in the chain pillars were unaffected by the mined-by of the longwall faces. The post-mining caliper survey found no deformations in the production4casings, and all the production casings passed pressure test. The shale gas wells resumed production after being interrupted for a short period during the mine-by.

Extended author information available on the last page of the article

Published online: 04 December 2025

Keywords Test well · Shale gas well · Longwall mining · Chain pillars · Casing deformations

1 Introduction

When gas wells penetrate through coal seams in the vicinity of longwall mining, they are subjected to longwall-induced subsurface movements, and casing deformations could occur. Excessive casing deformations could diminish casing integrity and allow high-pressure gas to leak into the longwall mine, potentially causing fires or explosions. Over the past decade, more than 1,800 shale gas wells have been drilled in the coal reserves of the Pittsburgh Coal Seam (Su and Zhang 2023). The influence of longwall mining on these shale gas wells has to be evaluated if they are located in longwall chain pillars or barrier pillars. To safely mine-by these shale gas wells, it is important to understand the location and amount of casing deformations induced by longwall mining and to take appropriate measures to maintain the casing integrity.

Longwall-induced casing deformations have been studied by Su (2016, 2017), Su et al. (2018, 2019), Scovazzo (2018), Zhang et al. (2020, 2022), and Zhang and Su (2021). Through instrumentation and numerical modeling techniques, these studies have greatly helped to understand overburden movements and casing deformations over longwall pillars. The first comprehensive instrumentation study conducted in 2013 and 2014 by CONSOL Energy, the Marcellus Shale Coalition, and the Pennsylvania Coal Association evaluated the effect of subsurface strata deformations on the gas well casings above the mining horizon by monitoring the response of test wells in the longwall abutment pillar. The study site was selected over the chain pillars between two 457-m wide longwall panels in a Pittsburgh coal seam longwall mine under 184-m depth of cover. The casing deformations on four test wells were measured with a 60-arm caliper after completion of each longwall panel. The detailed descriptions of the study site and data analysis were presented by Su (2016 and 2017) and Scovazzo (2018). The caliper surveys showed that the maximum horizontal displacement in all four test wells occurred at a depth of around 119 m at the same location (Su 2017). Scovazzo (2018) summarized the key findings from this instrumentation study which include: (1) casing deformation was identified in two settings: at the weak/strong rock contacts and within the Pittsburgh Coal Seam; (2) casing deformation was in response to ground movement occurring at weak/strong rock contacts and was above the well intersection with the angle of draw; (3) the most significant movement was found at the weak/strong rock contact on top of Limestone D with horizontal movements in all of the four test wells from 5.1 to 14.0 cm.

Zhang and Su (2021) modeled the comprehensively instrumented gas well study case to further investigate how geological factors influence the casing deformations of shale gas wells in longwall chain pillars under shallow cover. The modeling study found that casing deformations are primarily affected by rock layer thickness and the friction coefficient along the interface. The thicker the rock bed, the larger the casing deformation that could be induced by longwall mining. Large casing deformations can occur when the claystone interface is wet and the frictional coefficient is low. The frictional coefficient at the interface along a saturated claystone layer was found to be as low as 0.05 when a comparison was made between the predicted and measured casing deformations in the test well casings. A saturated claystone layer could be present at a shallow depth in a stream valley. High casing deformations near a stream valley are also confirmed by another instrumentation study by Su et al. (2019) on a test well in longwall chain pillars.

A few recent studies on unconventional gas wells in longwall pillars were also conducted by Liang et al. (2014, 2017) and Wang et al. (2013). Based on numerical modeling of hypothetical cases, these studies recognized that casing deformations would be potentially caused by horizontal slips along weak bedding planes and that thick beds and surface slopes would affect the amount of deformation. But without field measurement data, these modeling studies could not go beyond qualitative analysis.

To safely mine-by five shale gas wells in longwall chain pillars under medium cover, a test well was drilled in chain pillars in the same mining district to study the potential casing deformations under similar mining and geologic conditions. The casing deformations in the test well were measured with a 60-arm caliper after either side of the longwall panel was mined and also modeled with FLAC3D modeling technique. The knowledge of longwall-induced casing deformations gained from the test well was used to plan the mine-by of the real shale gas wells. The established FLAC3D model from the test well was used to predict intermediate casing deformations in the shale gas wells at the mine-by site. The study of the test well led to a successful shale gas well mine-by in which five shale gas wells in chain pillars survived longwall mining and resumed production after being interrupted during the period of mine-by. The post-mining caliper survey showed no casing deformations in the uncemented production casings.

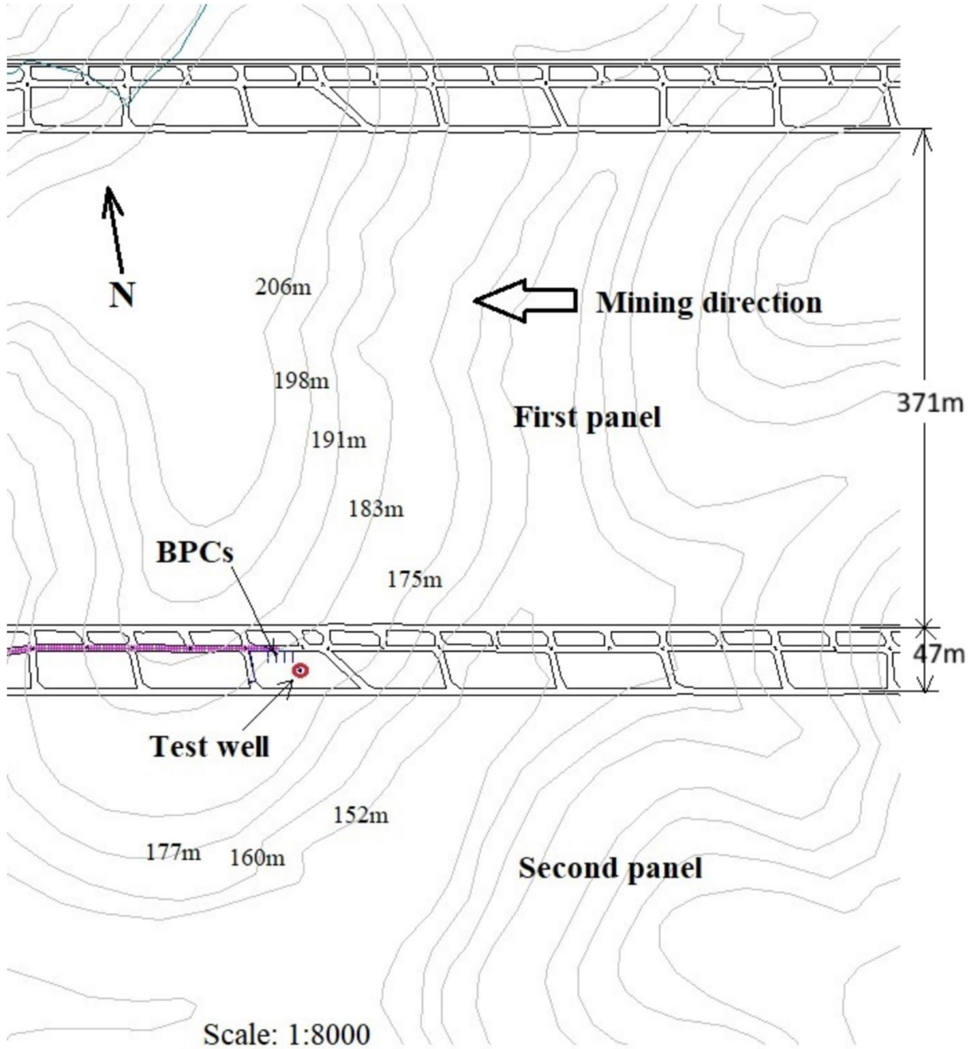

Fig. 1 Longwall panel layout and test well location with surface contour lines

1.1 Test Well Site Description

The study site was located over the chain pillars between two longwall panels in a West Virginia mine extracting coal from the Pittsburgh seam. Figure 1 shows the panel layout and test well location. A three-entry longwall gate-road system of 15-m × 32-m centers was employed at the mine. The longwall panels were 371-m wide, and the average mining height was approximately 2.1 m. The overburden depth at the test site was 186 m. Figure 1 also shows the location of the test well and underground instrumentation layout. The test well was drilled around the center of the abutment pillar of 27 m rib-to-rib, and the closest distance was 29 m from the test well to the first panel gob and 13 m to the second panel gob. The test well was drilled with a 31-cm hole to a depth of 207 m, about 30 m below the Pittsburgh seam. One 24-cm, J55 casing was installed in the hole to monitor casing deformations as the longwall panel on either side mined-by the test site. The thickness of the test well casing was 1 cm. The underground instrumentation consisted of four borehole pressure cells (BPCs) 6 m apart placed 8 m horizontally into the abutment pillar for measuring the abutment pillar pressure near the test well. The test site was passed first by first panel mining in August 2020 and then by second panel mining in March 2021. The test well casing was surveyed with a 60-arm caliper and a downhole video camera after each panel passed the test site for about 300 m.

The surface contour lines around the test site are also shown in Fig. 1. The surface around the test well is not flat but dips down about 30 m to the south and up about 23 m to the north. A creek is present about 150 m on the southeast side of the test well site. According to the coal seam elevations at the track entry, the coal seam has a dip of about 0.5 degrees to the southeast. As surface topography and coal seam dip influence surface and subsurface ground movements, they are considered in the numerical model.

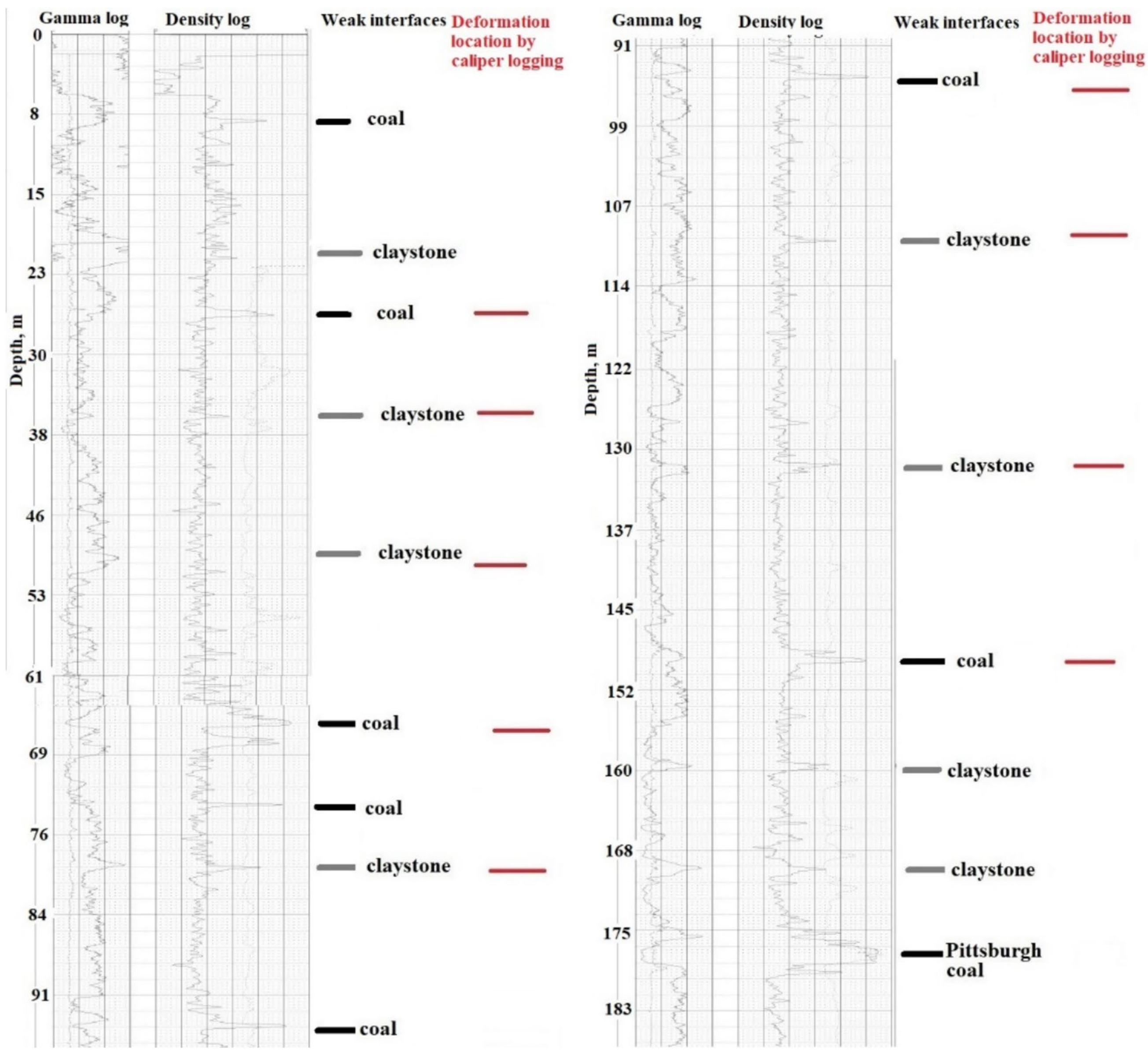

Fig. 2 Test site overburden geology and weak interface locations interpreted by correlating on-site gamma logs and a nearby core hole

Figure 2 shows the test site overburden geology and interface locations interpreted by correlating an on-site gamma log and a nearby core hole. The overburden geology over the test site is a typical Pittsburgh seam geology and is highlighted by many strong and weak rock interfaces along weak layers like claystone and coal. The claystone and coal interfaces are identified from the gamma log and density log. The weak interfaces represent the weak bedding between a weak layer and a relatively strong massive strata and are implemented in the FLAC3D model.

1.2 Numerical Model and Verification

Numerical modeling provides an effective tool for quantitatively assessing the influence of longwall mining on gas wells in longwall pillars. Researchers from the National Institute for Occupational Safety and Health (NIOSH) have developed FLAC3D modeling techniques to predict longwall-induced overburden movements and casing deformations (Zhang and Su 2021; Su et al. 2018, 2019; Zhang et al. 2020; and Tulu et al. 2017). In this study, the FLAC3D model (Itasca, 2017) was set up according to the geological conditions and longwall mining layouts around the test well site. Figure 3 shows the cross-sectional view of the FLAC3D model. The model included overburden from the Pittsburgh seam all the way up to the surface. The overburden lithology was from the lithology from the nearest core hole around the test well site. Table 1 shows the rock properties used in the model. The weak bedding interface locations were determined from the on-site gamma logs. The surface slope over the longwall panel was also modeled. The longwall caving zone was modeled by strain-hardening material implemented by the "FISH" scripting language in FLAC3D (Itasca, 2017). The overburden strata above the caving zone were modeled with ubiquitous joint material, and the coal seam, immediate roof, and floor were modeled with Mohr–Coulomb materials. In situ horizontal stresses were applied in the model with the maximum horizontal stress of three times the vertical stress along the panel and the minimum horizontal stress of two times the vertical stress across the panel. The test well casing was modeled in accordance with its size and mechanical properties. To accurately model the casing deformation, the mesh size around the test well was gradually reduced. At the test well casing, the mesh size was reduced to a minimum of 0.5 cm. Table 2 shows the mechanical properties of the test well casing. The steel casings were modeled with von Mises material, and the cement fillings were modeled with Mohr–Coulomb material. The casing was installed in the model before the longwall gate entries were developed.

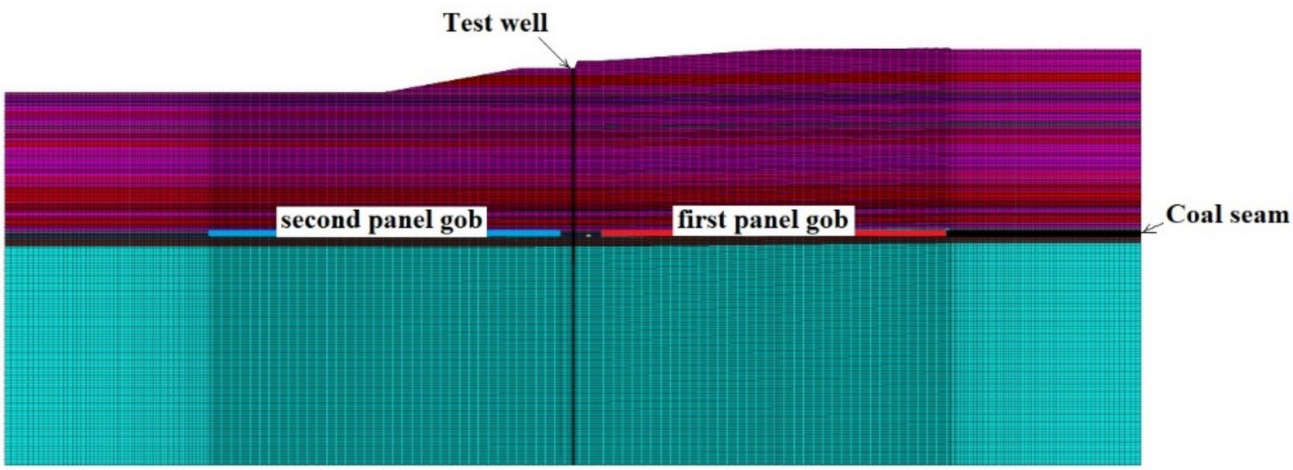

Fig. 3 Sectional view of the FLAC3D model

Table 1 Rock properties used in the model

Rock type	Young's modulus, MPa	Poisson's ratio	Cohesion, MPa	Internal friction angle, degrees	Tensile strength, MPa
Coal	2,070	0.30	1.9	28	0.3
Claystone	2,900	0.3	1.9	28	0.3
Shale	11,600	0.25	11.7	35	4.5
Sandy shale	11,600	0.25	11.7	35	4.5
Sandstone	11,600	0.25	17.9	35	6.9
Limestone	17,400	0.22	15.9	35	6.1
shaley Limestone	17,400	0.22	14.5	38	5.9
shaley Sandstone	15,000	0.22	11.7	38	4.8
Siltyshale	11,600	0.25	11.7	32	4.2

Table 2 Mechanical properties of the test well casing

Test well component	Outside diameter, cm	Wall thickness, cm	Young's modulus, MPa	Poisson's ratio	Yield strength, MPa
Test casing	24.4	1.0	2.0×10^5	0.3	345.0
Cement filling	31.0	6.5	6.9×10^3	0.25	13.8

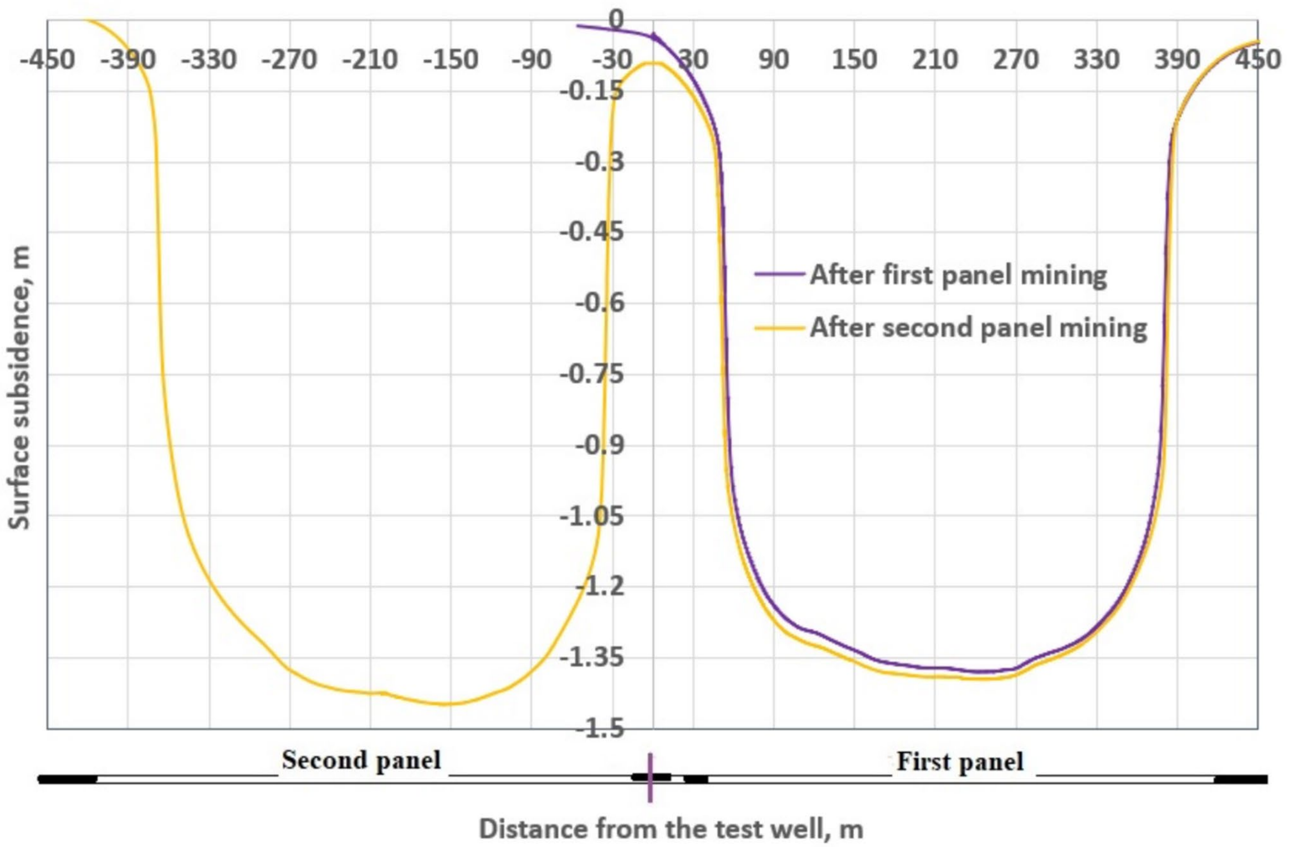

Fig. 4 Predicted final surface subsidence across the chain pillars and two longwall panels after first and second panel mining

The FLAC3D model for the study site is set up with site-specific mining and geologic conditions, and surface subsidence and pillar pressure are used to verify the model. Figure 4 shows predicted final surface subsidence across the test well and the longwall panels after each panel is completed. The predicted final subsidence curve is almost flat around the panel center but is asymmetrical due to the presence of surface slope above the panel. The model predicts a maximum subsidence of about 1.31–1.34 m around the panel center. At the gas well location, the predicted surface subsidence is about 3.0 cm after first panel mining and 9.7 cm after second panel mining. The subsidence is small at the test well site because the overburden is shallow.

Figure 5 shows the predicted vertical stress distribution across the chain pillars at the coal seam horizon after first and second panel mining. At the coal seam horizon, the gas well is mainly influenced by the longwall-induced vertical stress in the coal pillar near the well. The predicted pillar pressure increases at the test well location are about 2 MPa after first panel mining and 4 MPa after second panel mining. A longwall-induced pillar pressure increase near the test well was measured by borehole pressure cells (BPCs) as the first panel mined-by the test site, and the measured pillar pressure increase is shown in Fig. 6. The BPCs were installed horizontally 8.2 m into the abutment pillar from the track entry. The measured pillar pressure increase was 4.1 MPa after first panel mining. The predicted pillar pressure increase at the BPC location was 4.3 MPa after first panel mining. By comparison, the model reasonably predicts the longwall-induced vertical stress around the chain pillars.

1.3 Comparison of Predicted and Measured Casing Deformations

The model predicted horizontal displacement along the test well casing after first panel mining as shown in Fig. 7. After first panel mining, the casing moves towards the first panel gob. At the surface, the casing moves about 2 cm towards the

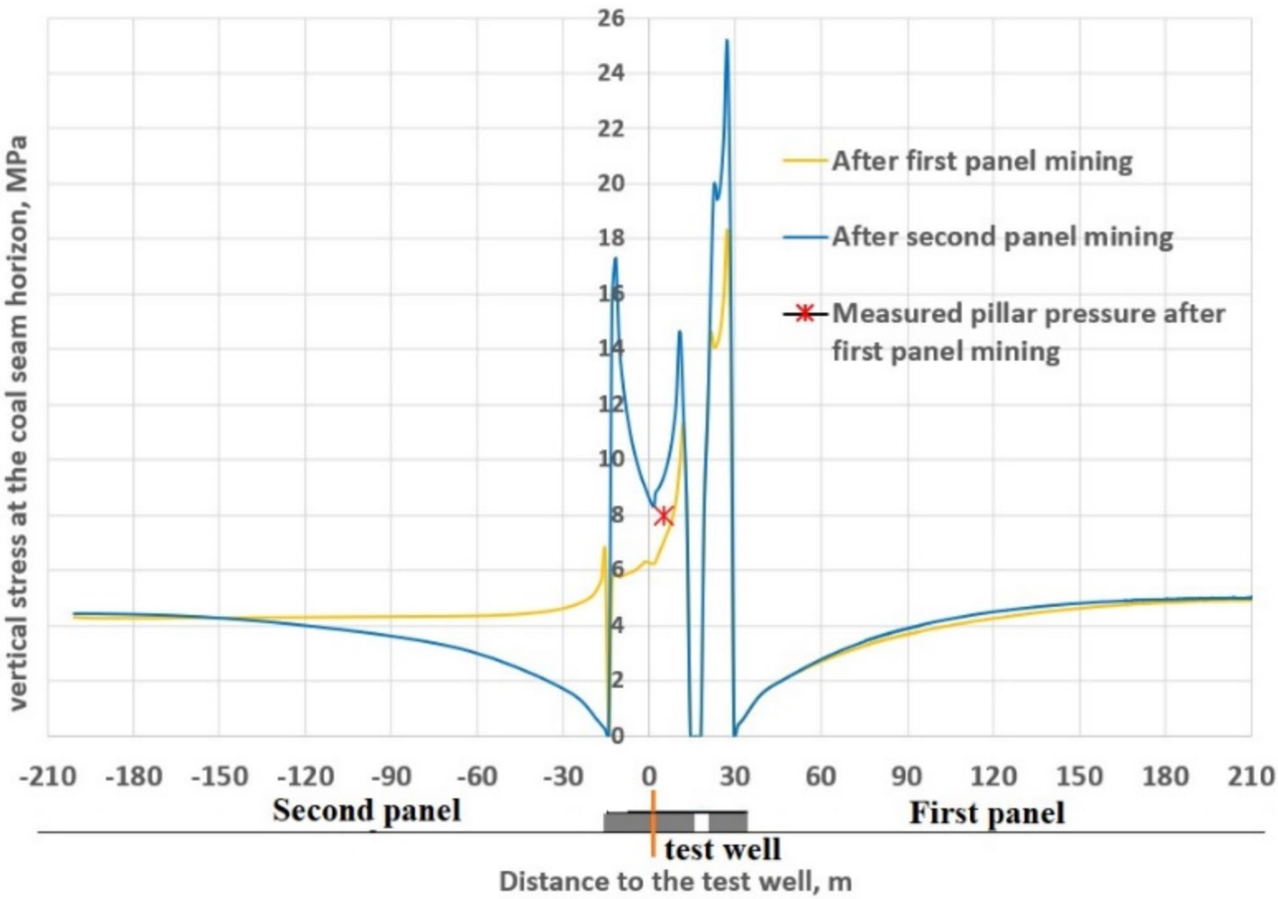

Fig. 5 Predicted vertical stress distribution at the coal seam horizon and measured pillar pressure near the test well

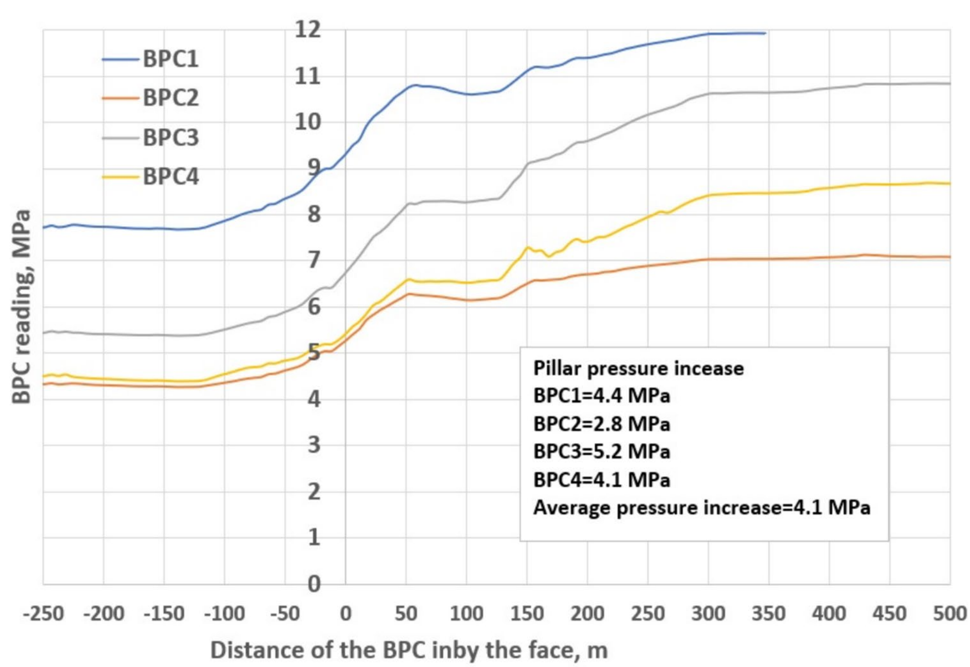

Fig. 6 Measured pillar pressure increases by BPCs with first panel mining

Fig. 7 Predicted horizontal displacement and deformation locations along the test well casing after first panel mining

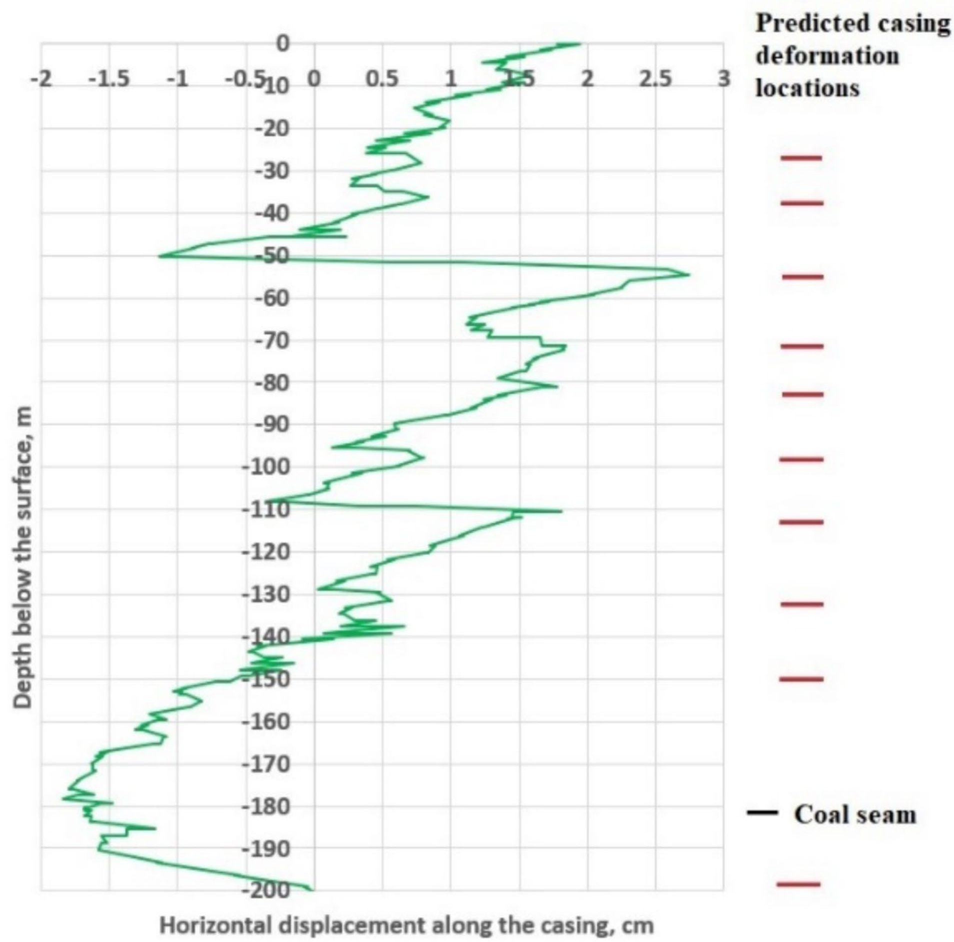

gob. In the subsurface, the casing is also subjected to relative horizontal displacements or shear displacements at interface locations. Casing deformations are caused by relative horizontal displacements along strong/weak rock interfaces. From the horizontal displacement curve, the casing deformations are predicted at the locations shown in Fig. 7. With second panel mining, the casing moves towards the second panel gob. Figure 8 shows the predicted horizontal displacement along the test well casing after second panel mining. The displacement curve indicates that casing deformations occur at the same locations after second panel mining.

The casing deformations were measured by 60-arm caliper logging after first and second panel mining. Figure 9 shows the measured casing inside diameter changes after first panel mining. The nominal casing inside diameter for the 9–5/8-in casing is 22.4 cm. This figure shows that the casing diameters reduced when the casing deformed. Casing deformations were detected at ten locations below the surface. The largest diameter reduction was 6.8 cm at 51 m below the surface, and the diameter reduction at other locations was less than 1 cm.

The changes of measured and predicted casing diameters after first panel mining are summarized in Table 3. The minimum casing diameter change is estimated from the predicted relative horizontal displacement multiplied by a factor of 1.4. This factor is determined by analyzing the caliper-logging data. From the caliper survey, the casing becomes ovalized after being deformed. The deformed casing along the minimum diameter tends to be oriented perpendicular to the longwall mining direction. A diameter increase along the mining direction is also measured by caliper logging, but the casing minimum diameter change is used for analyzing casing deformation because the diameter reduction across the panel is the result of shear displacement. Under the shear displacement at an interface across the longwall mining direction, the casing deforms on two sides opposite to each other. One side is the active side subjected to active force, and the other side is the reactive side. The deformation on the active side generally represents the relative horizontal displacement along the interface. This was also illustrated by Zhang et al. (2023) through modeling casing deformations at an interface. Based on the results of the caliper survey on the test well, the deformation at the reactive side is about

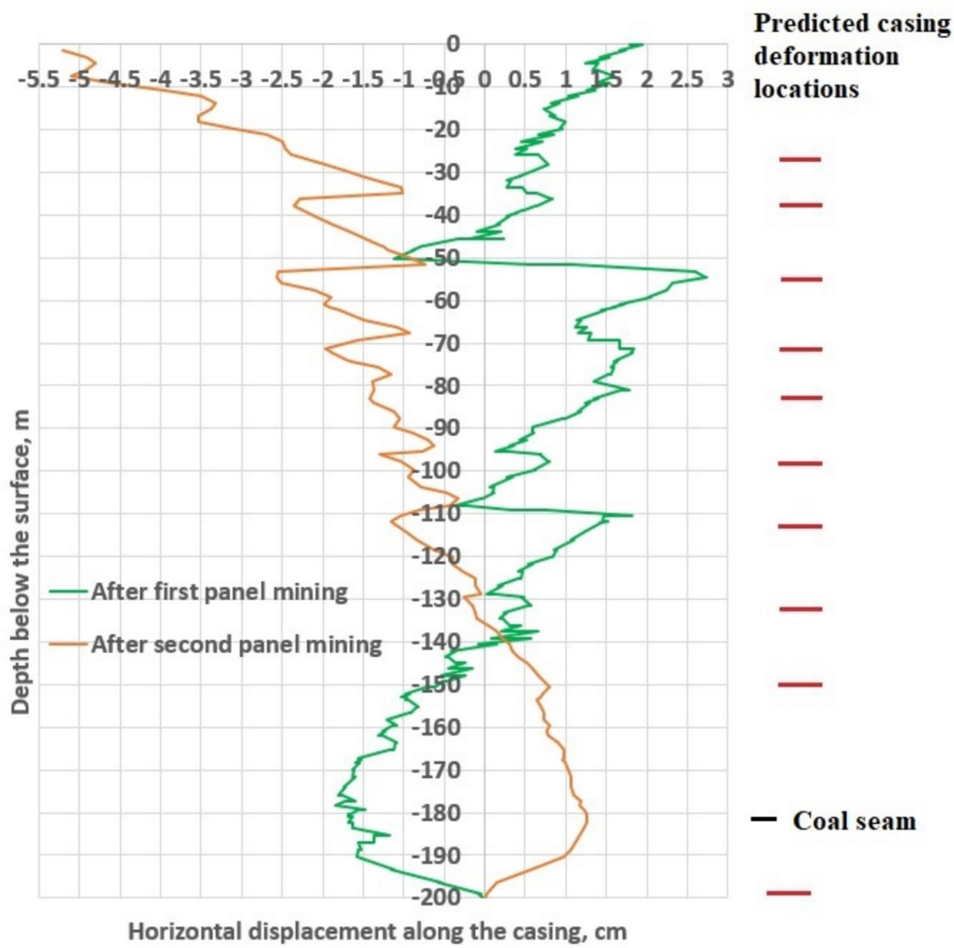

Fig. 8 Predicted horizontal displacement and deformation locations along the test well casing after second panel mining

40% of the amount at the active side. The deformation at each side causes a radius change in the casing. The sum of the radius changes is the casing minimum diameter change to be estimated at about 1.4 times the predicted horizontal relative displacement. For comparison, the predicted casing diameter changes are also plotted in Fig. 9, which shows that the prediction and measurement are in reasonable agreement in both locations and magnitudes.

Figure 10 shows the measured casing minimum diameter changes after second panel mining. The measured and predicted casing diameter changes after second panel mining are summarized in Table 4. As overburden moves towards the second panel, additional relative horizontal displacement occurs at the same interfaces but in the opposite direction. The total casing diameter change is accumulative. The measurements show that the casing deformations remain at the same locations. The maximum diameter reduction is still at the horizon 51 m below the surface, but the magnitude increases from 6.8 to 8.2 cm. The second largest diameter reduction is 3.2 cm which occurs at 110 m below the surface. The casing diameter reductions at other locations increase slightly after second panel mining. The predicted casing diameter changes after second panel mining are also plotted in Fig. 10, and by comparison, the prediction reasonably agrees with the measurement. The casing deformation locations are compared with the overburden geology at the test well site as shown in Fig. 2. The comparison indicates that all the casing deformations occurred at the weak claystone and coal interfaces. Figure 11 shows predicted deformation locations in comparison with caliper-detected deformation locations. The predicted deformation locations are generally in good agreement with the measured deformation locations.

The test well casing was also surveyed with a downhole video camera after first panel was mined. Casing deformations were observed at two locations: 51 and 110 m below the surface. Figure 12 shows the casing deformations observed with the downhole camera at 51 and 100 m below the surface. At the 51-m depth, a 6.8-cm casing diameter reduction was detected by the 60-arm caliper logging, and the casing is bulged with shear deformation. At the 110-m depth, about a 1-cm casing diameter reduction was detected by the 60-arm caliper logging, and an ovalized shape and a small amount of shearing can be seen.

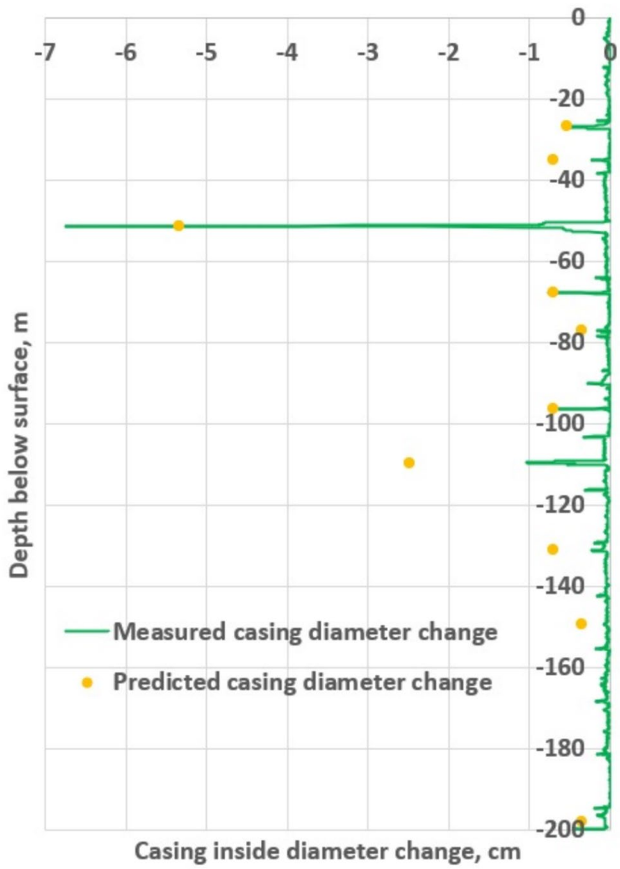

Fig. 9 Measured and predicted casing minimum inside diameter changes after first panel mining

Stresses in the casing induced by ground movements include three components: vertical, horizontal, and shear. The combination of all the stress components can be represented by von Mises stress. The von Mises stress gives an indication of the casing's stress level compared to its strength capacity and can be used to predict casing yielding. Figure 13 shows the von Mises stress and yielding locations in the intermediate casing. This figure shows that casing deformations occur at locations with high von Mises stress. Above the coal seam, von Mises stress exceeds the casing strength at four locations at the weak interfaces. At the coal seam horizon, the von Mises stress reaches the casing strength after second panel mining because of the higher abutment pressure in the chain pillars.

1.4 Development of Casing Deformations at the Interface

At the weak rock interface, casing deformations are induced by the relative horizontal displacement or shear displacement along the interface, and this displacement can be captured by the multi-finger caliper logging. The results of the 60-arm caliper logging in this study have shown that the casing deformation initiates at the bottom of the claystone layer after first panel mining and then propagates upward towards the top of the claystone after second panel mining. The amount and the extent of the deformation depend on the amount of relative horizontal displacement along the interface. By caliper logging, the casing deformation at the interface is confined within the thickness of the weak layer. Figure 14 shows the casing deformations at a 51-m depth after first and second panel mining. The images are rendered from the caliper logging data. According to the core log and gamma logs, the deformations occurred at a 0.9-m claystone layer underlain by a massive limestone layer. After first panel mining, the casing deformations mainly occurred within about 0.3 m of the claystone layer at the bottom. The deformations developed at two opposite sides of the casing is an indication that shear displacement took place along the interface. The white arrows in Fig. 14 indicate shearing directions. The shear displacement is not apparent in the image because the caliper arms were not centralized when passing the interface with a shear displacement. After second panel

Table 3 Comparison between predicted and measured casing deformations after first panel mining

Depth below surface, m	Predicted relative displacement, cm	Predicted casing diameter change, cm	Measured casing diameter change, cm	Error, cm
27	0.38	0.53	0.48	0.05
35	0.51	0.71	0.20	0.51
51	3.81	5.33	6.80	1.47
68	0.51	0.71	0.74	0.03
77	0.25	0.36	0.18	0.18
96	0.51	0.71	0.64	0.07
110	1.78	2.49	1.02	1.47
131	0.51	0.71	0.20	0.51
149	0.25	0.36	0.08	0.28
200	0.25	0.36	0.46	0.10

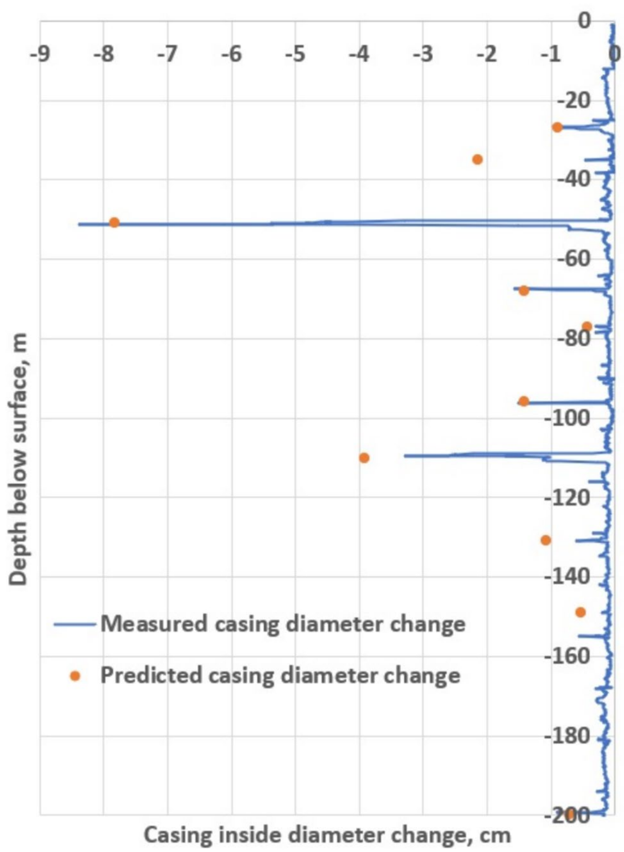

Fig. 10 Measured and predicted casing minimum inside diameter changes after second panel mining

mining, the deformation propagated upward and extended to the whole claystone layer. As the deformation is induced by shear displacement at the claystone interface, the extent of the deformation is restricted within the claystone layer. The growth of the deformation zones after second panel mining is associated with time-dependent deformation of the claystone and possible claystone weakening due to water saturation.

Figure 15 shows the casing deformations at a 0.6-m claystone layer at a 110-m depth after first and second panel mining. This figure shows the deformation develops at a 110-m depth in a similar manner as at a 51-m depth. It clearly indicates that the deformation initiates at the active panel side, at which the deformation is larger. Figure 15 also shows that the extent of the deformation is restricted within the thickness of the claystone layer.

1.5 A Successful Shale Gas Well Mine-by Following the Test Well Study

Both modeling and measurement of the casing deformations in the test well showed that the maximum intermediate casing deformation was less than 6.8 cm after first panel mining and less than 8.2 cm after second panel mining. The study of longwall-induced deformations in the test well provided a good understanding about the potential casing deformations that could be induced by longwall mining in the shale gas wells in the chain pillars under similar conditions. Since the maximum deformation in the test well casing was less than the standard annulus of 8.4 cm between production and intermediate casings of shale gas wells, it is reasonable to assume that the production casing in actual shale gas wells would not be affected by longwall-induced deformations in the intermediate casing if the production casing is left uncemented. This assumption was verified by a mine-by case with five shale gas wells in the chain pillars in the same mining district. The shale gas wells were constructed with typical casing design, but the production casings were uncemented. The casing deformations were predicted by the FLAC3D model established with the test well study and were surveyed by a multi-finger caliper. No deformations

Table 4 Comparison between predicted and measured casing deformations after second panel mining

Depth below surface, m	Predicted relative displacement after second panel mining, cm	Predicted accumulative relative horizontal displacement, cm	Predicted casing diameter change, cm	Measured casing diameter change, cm	Error, cm
27	0.25	0.64	0.89	0.81	0.08
35	1.02	1.52	2.13	0.36	1.77
51	1.78	5.59	7.82	8.20	0.38
68	0.51	1.02	1.42	1.71	0.29
77	0.05	0.30	0.43	0.18	0.25
96	0.51	1.02	1.42	1.62	0.20
110	1.02	2.79	3.91	3.20	0.71
131	0.25	0.76	1.07	0.46	0.61
149	0.13	0.38	0.53	0.10	0.43
200	0.25	0.51	0.71	0.82	0.11

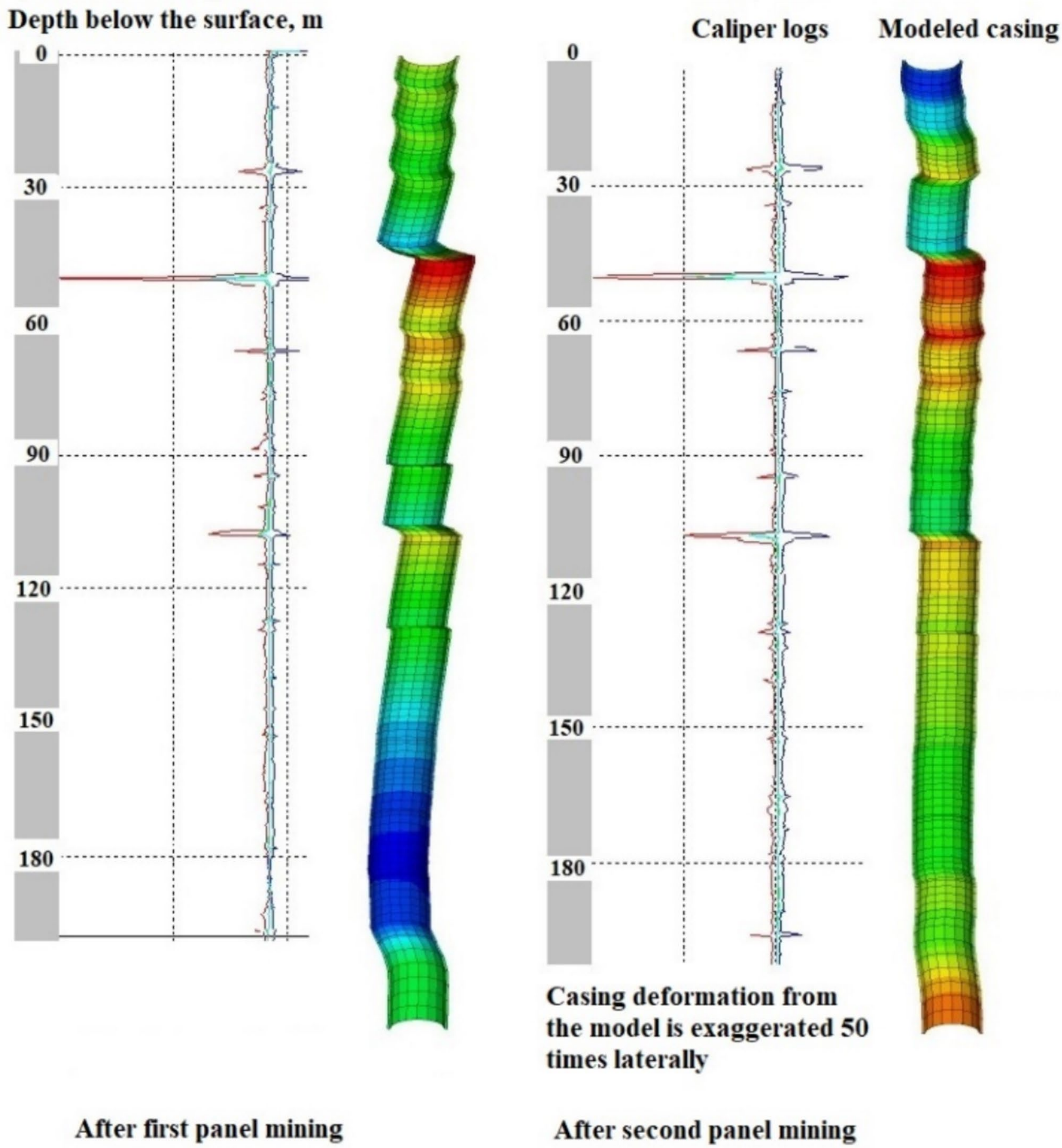

Fig. 11 Comparison of modeled and caliper-surveyed casing deformations: **a** Top-down view of the deformation location from the 51-m depth. **b** Top-down view of the deformation location from the 110-m depth

were predicted and measured in the uncemented production casings.

The five shale gas wells were located in the chain pillars between two adjacent longwall panels in the Pittsburgh Coal Seam. Figure 16 shows the pillar layout and gas well locations. The longwall panels were developed with a three-entry system with a total chain pillar width of 52 m center-to-center. The longwall panels were 366-m wide with a mining height of 2.1 m. The overburden depth at the well pad was 204 m. Five shale gas wells were located around the center of an abutment pillar 79-m long and 32-m wide rib-to-rib. The wells were named 1H, 2H, 3H, 6H, and 7H. The setback

Fig. 12 Casing deformation at 51-m and 110-m depths viewed with downhole camera

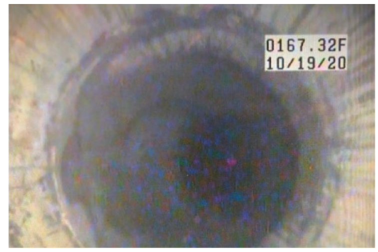

a. Top-down view of the deformation location from the 51-m depth.

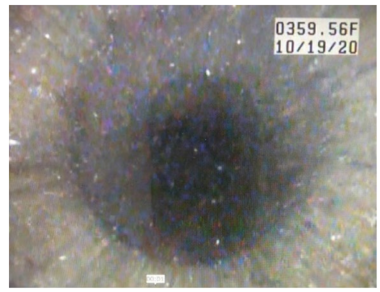

b. Top-down view of the deformation location from the 110-m depth.

Fig. 13 Von Mises stress in the test well casing after first and second panel mining

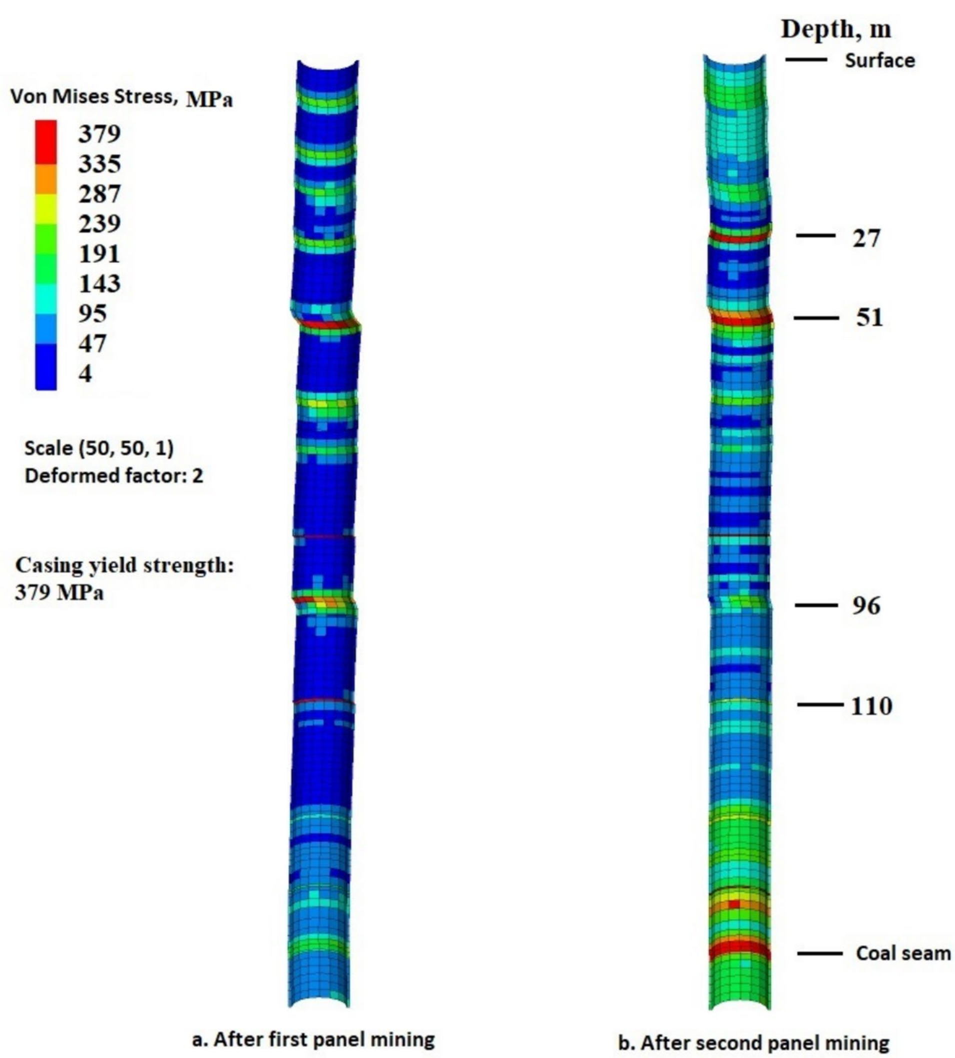

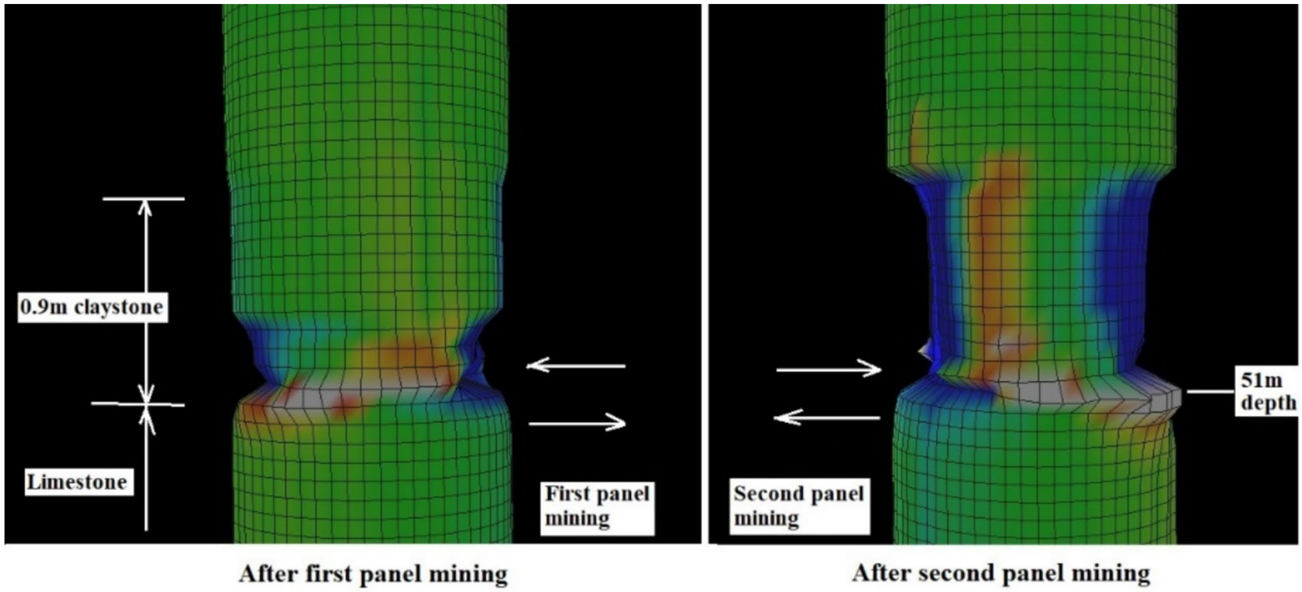

Fig. 14 Development of casing deformation at 51-m depth after first and second panel mining (white arrows indicate shearing directions)

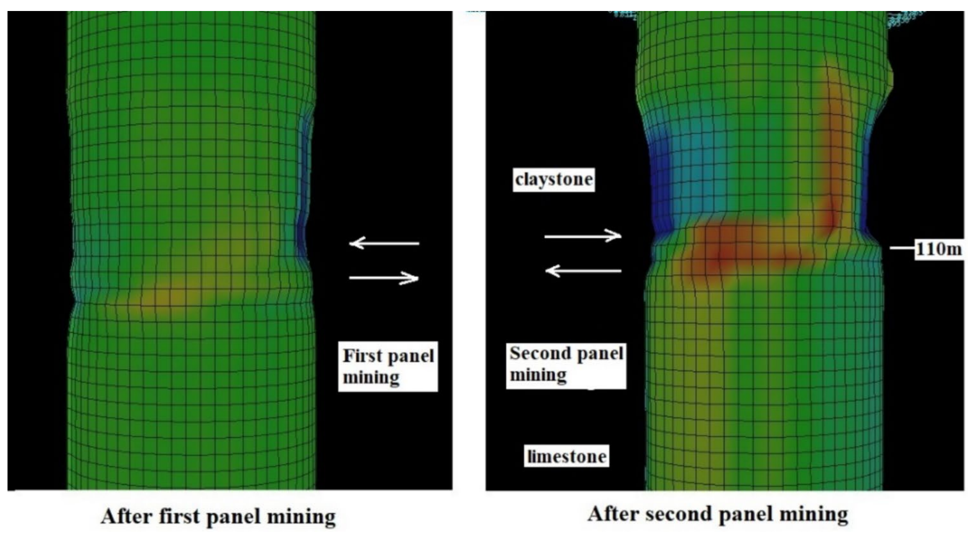

Fig. 15 Development of casing deformation at 110-m depth after first and second panel mining (white arrows indicate shearing directions)

distance from the gas wells was 30.5 m to the first panel gob and 16.5 m to the second panel gob. The first panel mined-by the gas wells in March 2022, and the second panel mined-by was in October 2022.

A FLAC3D model was set up according to site-specific geologic conditions at the shale gas well pad. The model was used to predict the casing deformations in the intermediate casing of the shale gas wells. Figure 17 shows the predicted horizontal displacements along the intermediate casing after first and second panel mining. The predicted relative horizontal displacements and casing diameter reductions after first and second panel mining are summarized in Table 5. The predicted maximum casing deformation is 3.74 cm at a 79-m depth after first panel mining and 5.59 cm at the same depth after second panel mining. As the maximum casing deformation is less than the open annular space of 8.4 cm between the production and intermediate casing, no deformation in the production casing was expected after first and second panel mining. The FLAC3D predictions and the experience of the test well casing deformations greatly help to plan the shale gas well mine-by. The five shale gas wells were unaffected during mine-by of the longwall faces. No deformation was detected in the uncemented production casings by the post-mining multi-finger caliper surveys, and all the production casings passed pressure test. The gas wells resumed production after being interrupted for a short period during the mine-by.

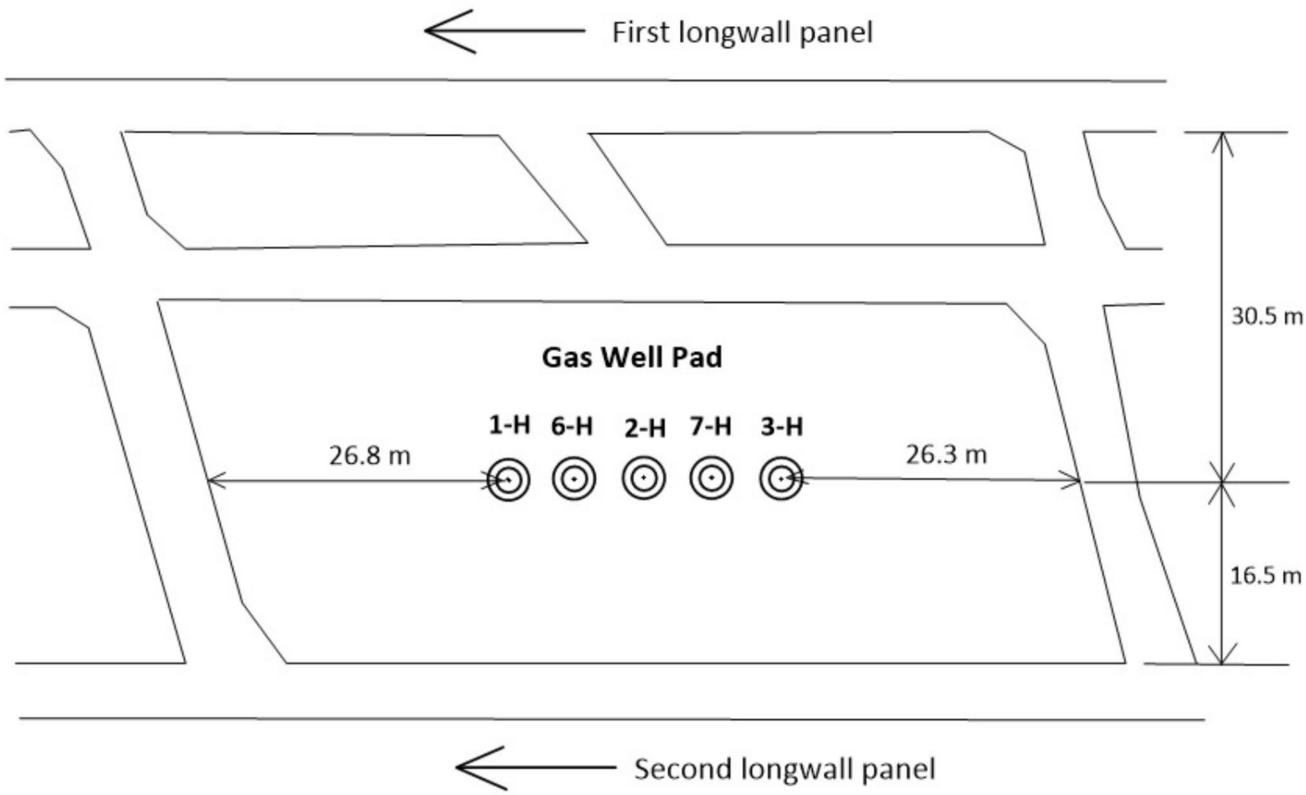

Fig. 16 Longwall pillar layout and shale gas well locations

2 Limitations

The findings in this manuscript are based on a test well in the Pittsburgh Coal Seam with site-specific overburden geology and mining conditions. Casing deformations are affected by many factors such as overburden depth, surface topography, interface friction, presence of thick beds, and gas well setback distance. Larger casing deformations than predicted and measured in this study could occur if a stream valley, very thick massive strata, larger strata dip, and a weak claystone floor are present. In this study, overburden depth, stream valley, and setback distance are included in the model, but thick beds, large strata dip, and weak claystone floor are not accounted for. The overburden depths in this study are considered shallow to medium and do not represent all the mining depths in the Pittsburgh seam. Under deeper cover, casing deformations could potentially occur at the coal seam horizon, and this concern needs to be further addressed. Even though casing deformations did not occur in the uncemented production casings in this case, it does not mean that uncemented casings can always eliminate casing deformations under similar overburden depth. The presence of a major stream valley near the gas well site and the potential time-dependent deformation of a weak claystone in the floor could cause casing deformations under shallow and medium cover.

Since this study represents only two gas well sites at the cover depths of 186 and 204 m, more data at similar cover gas well sites are needed to confirm that the conclusions found from this study are applicable to different site conditions. The FLAC3D simulations are purely modeling predictions, within the variance of the variables and parameters used, and need to be validated by actual field data. Similar shallow and medium cover site data would need to be collected to enhance the data population to make the results statistically valid.

3 Conclusion

In this study, a test well was drilled in the chain pillars between two adjacent longwall panels to investigate how casing deformations could occur under the influence of longwall-induced subsurface ground movements. Casing deformations were measured by a multi-finger caliper and predicted by the FLAC3D modeling technique. The FLAC3D model established with the test well study was used to predict casing deformations for a shale gas well mine-by case in the same mining district. Conclusions

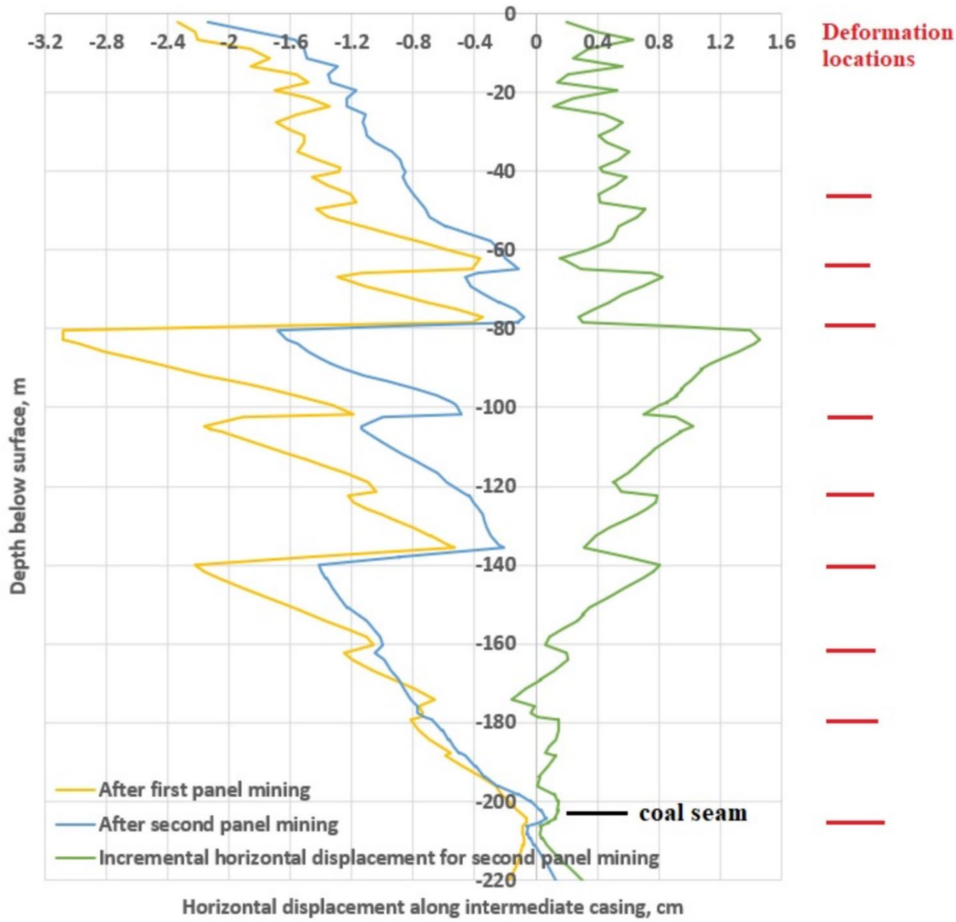

Fig. 17 Predicted horizontal displacement along intermediate casing after first and second panel mining

Table 5 Predicted casing deformations in the intermediate casing after first and second panel mining

Depth below surface, m	First panel mining		Second panel mining	
	Predicted relative horizontal displacement, cm	Predicted casing diameter change, cm	Predicted accumulative relative horizontal displacement, cm	Predicted casing diameter change, cm
48	0.25	0.35	0.25	0.71
64	1.02	1.43	0.46	2.06
79	2.67	3.74	1.27	5.59
105	1.02	1.43	0.25	1.78
122	0.20	0.28	0.23	0.61
137	1.78	2.49	0.51	3.20
162	0.15	0.21	0.38	0.38
174	0.13	0.18	0.38	0.36
202	0	0	0.38	0.18

derived from comparing field measurements and FLAC3D modeling predictions of casing deformations are as follows:

- Casing deformations occurred at distinct weak/strong rock interfaces due to relative horizontal displacements along the interfaces. Casing deformations occurred at the same locations for both first and second panel mining.
- Casing deformations increased slightly after second panel mining as the relative horizontal shear displacements shifted in the opposite direction. The largest casing

deformation in the test well was 8.2 cm measured at 51 m below the surface after second panel mining.

- Casing deformations were confined within the thickness of weak claystone layers. The casing deformation zone at a claystone layer at the 51-m depth in the test well increased from 0.3 m after first panel mining to the extent of the claystone thickness of 0.9 m after second panel mining.
- Casing deformations in the five shale gas wells in longwall chain pillars in the same mining district were predicted using the established FLAC3D model from the test well study. The predicted maximum casing deformation in the intermediate casing of the shale gas wells was 3.74 cm at a 79-m depth after first panel mining and 5.59 cm at the same depth after second panel mining. As the maximum casing deformation was less than the open annular space of 8.4 cm between the production and intermediate casing, no deformations in the production casing were expected.
- With uncemented production casings, the five shale gas wells in chain pillars were unaffected by the mine-by of the longwall faces. No deformation was detected in the uncemented production casings by the post-mining multi-finger caliper surveys, and all the production casings passed pressure test. The shale gas wells resumed production after being interrupted for a short period during the mine-by.

Author Contributions Peter Zhang performed FLAC3D modeling, analyzed field measurement data, and wrote the manuscript. Daniel Su provided technical advice on FLAC3D modeling and the interpretation of the caliper survey data. Bo Hyun Kim provided technical advice on FLAC3D modeling. Evan Midler helped to plan the underground instrumentation and provided geologic information. All authors reviewed and approved the final manuscript.

Funding No funding was received for conducting this study.

Data availability Not applicable.

Declarations

Conflict of Interest The authors have no relevant financial or non-financial interests to disclose.

Disclaimer The findings and conclusions in this report are those of the author(s) and do not necessarily represent the official position of the National Institute for Occupational Safety and Health (NIOSH), Centers for Disease Control and Prevention (CDC). Mention of any company or product does not constitute endorsement by NIOSH.

References

ITASCA Consulting Group, Inc. 2017. FLAC3D, Version 6.0, User's Guide

Liang S, Elsworth D, Li X, Fu X, Sun B, Yao Q (2017) Key strata characteristics controlling the integrity of deep wells in longwall mining areas. Int J Coal Geol 132:23–36

Liang S, Elsworth D, Li X, Yang D (2014) Topographic influence on stability of gas wells penetrating longwall mining areas. Int J Coal Geol 172:31–42

Scovazzo V (2018) Mining effects on gas and oil wells pad NV-35 field experiment field monitoring. In *Proceedings of the 37th International Conference on Ground Control in Mining*. Morgantown, WV: West Virginia University, pp. 30–43

Su DWH (2017) Effects of longwall-induced subsurface deformations on the mechanical integrity of shale gas wells drilled over a longwall abutment pillar. *2017 SME Annual Meeting*, Feb. 19–22, 2017, Denver. CO Preprint 17–051:1–6

Su DWH, Zhang P (2023) Longwall-induced deformations and shale gas well casing stresses: Engineering principles. In *Proceedings of the 57th U.S. Rock Mechanics Geomechanics Symposium*, Atlanta, GA, June 26–28, 2023, p.9

Su DWH, Zhang P, Van Dyke M, Minoski T (2018) Effects of longwall-induced subsurface deformations on shale gas well casing stability under deep covers. In *Proceedings of the 37th International Conference on Ground Control in Mining*. Morgantown, WV: West Virginia University, pp. 63–70

Su DWH, Zhang P, Dougherty H, Van Dyke M, Minoski T, Schatzel S, Gangrade V, Watkins E, Addis J, Hollerich C (2019) Longwall-induced subsurface deformations and permeability changes – Shale gas well casing integrity implication. In *Proceedings of the 38th International Conference on Ground Control in Mining*. Morgantown, WV: West Virginia University, pp. 49–59

Su DWH (2016) Effects of longwall-induced stress and deformation on the stability and mechanical integrity of shale gas wells drilled through a longwall abutment pillar. In *Proceedings of the 35th International Conference on Ground Control in Mining*. Morgantown, West Virginia, pp. 119–125

Tulu IB, Esterhuizen GS, Mohamed KM, Klemetti TM (2017) Verification of a calibrated longwall model with field measurements. In *Proceedings of the 51st US Rock Mechanics/Geomechanics Symposium*, 25–28 June 2017. San Francisco

Wang Y, Watson R, Rostami J, Wang JY, Limbruner M, He Z (2013) Study of borehole stability of Marcellus shale wells in longwall mining areas. J Pet Explor Prod Technol 4:59–71

Zhang P, Su D (2021) FLAC3D modeling evaluation of the comprehensive NV-35 gas well pillar study. In *Proceedings of the 55th US Rock Mechanics/Geomechanics Symposium*, 20–23 June 2021. Texas

Zhang P, Dougherty H, Su D, Trackemas J, Tulu B (2020) Influence of longwall mining on the stability of gas wells in chain pillars. Int J Min Sci Technol 30(1):3–9

Zhang P, Su D, Van Dyke M, Dougherty H (2022) Shale gas well casing deformation in longwall chain pillars under deep cover – Field measurement and numerical modeling. In *Proceedings of the 41st International Conference on Ground Control in Mining*, Canonsburg, PA, July 26–28, 2022

Zhang P, Su D, Van Dyke M, Kim BH (2023) A case study of shale gas well casing deformation in longwall chain pillars under deep cover. *57th U.S. Rock Mechanics Geomechanics Symposium*, Atlanta, GA, June 26–28, 2023, pp.9

Authors and Affiliations

Peter Zhang[1] · **Daniel Su**[1] · **Bo Hyun Kim**[2] · **Evan Midler**[3]

✉ Peter Zhang
nmb2@cdc.gov

1 NIOSH, Pittsburgh Mining Research Division, 626 Cochrans Mill Road, Pittsburgh, PA 15236, USA

2 NIOSH, Spokane Mining Research Division, 315 E. Montgomery Avenue, Spokane, WA 99207, USA

3 Alliance Coal, LLC, 184 Schoolhouse Road, Valley Grove, WV 26060, USA